Supplementary Information

Biocompatible Ni(II) Complex as an Amyloid Sensor for Human $PrP_{106\text{-}126}$ Fibrillar Aggregates

Rajat Saini,[a] Rahul Chauhan,[a] Sain Singh,[a] Saakshi Saini,[b] Govinda R. Navale,[a] Abhishek Panwar,[c] Prashant Kukreti,[a] Imtiaz Ahmed,[a] Partha Roy,[b] and Kaushik Ghosh [a,b]*

[a]Department of Chemistry, Indian Institute of Technology Roorkee, Roorkee, 247667, India.

[b]Department of Biosciences and Bioengineering, Indian Institute of Technology Roorkee, Roorkee, 247667, India.

[c]Department of Chemistry, National Institute of Technology Manipur, Langol-795004, Imphal West, Manipur, India

E-mail: kaushik.ghosh@cy.iitr.ac.in and kg@bt.iitr.ac.in

Table of Contents

Experimental details	3
General synthesis	3
General characterization	3
Synthesis schemes	3
X-ray crystallography, Crystal data, and refinement parameters	5
Preparation of $PrP_{106-126}$ fibrils	12
Job's Plot Analysis	12
Benesi-Hildebrand Plot	12
Evan's Method	13
Detection of $PrP_{106-126}$ aggregates in neuronal HT-22 cells	13
Molecular Docking	14
MALDI-TOF MS	14
Quantum Yield determination of KRS-1	15
Supplementary Figures	16
References	29

Experimental details

General Synthesis

All chemicals used were of laboratory grade and purchased from Sigma-Aldrich (Merck) and were used without further purification. The reaction was monitored by thin-layer chromatography using reversed-phase aluminium TLC plates (Merck, TLC Silica gel RP-18 F254s).

General Characterization

The medium used for all photophysical experiments was phosphate-buffered saline (PBS; pH 7.4). The concentrated stock solution (5 mM) was prepared in DMSO (Molecular Biology grade, Sigma Aldrich) and diluted to the required concentration in PBS for further experiments. In every experiment, the DMSO concentration was 0.5% volume/volume. The UV-Vis spectra were recorded using a Shimadzu UV-2600 spectrophotometer. The fluorescence spectra were recorded using a Synergy Biotek Citation 3 multi-mode plate reader and a Horiba fluorescence spectrophotometer.

Synthesis schemes

Synthesis of diformyl precursor of 4-tertbutyl phenol

The synthesis of diformyl precursor of 4-tertbutyl phenol was performed by the reported procedure.[1]

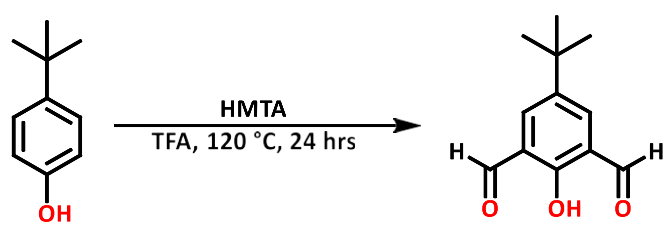

Synthesis of Bis-Benzothiazole based ligand (HL)

The Bis-Benzothiazole ligand has been synthesized in the literature.[2] However, we utilized a more facile and unique method to synthesize this ligand. The Bis-Benzothiazole-based ligand (HL) was synthesized by a one-pot 2:1 condensation reaction of 2-aminothiophenol with 4-tertbutyl-2,6-diformylphenol in dimethyl sulphoxide (which acts as both solvent and oxidizing agent). To a Round Bottom (RB) flask, 100 mg (0.4854 millimoles) of diformyl precursor and

121.53 mg (0.9708 millimoles) of 2-aminothiophenol were added in 25 mL of dimethyl sulphoxide and refluxed at 110°C for 3 hours. The orange crystalline solid appeared in the reaction mixture and was filtered and cooled to room temperature. Yield (92%), Melting point (245°C). The ligand was characterized by FT-IR, UV-visible, and NMR. IR data (KBr, *ν* cm^{-1}): ~3,445 *ν*(OH), 3,058 *ν*($C\text{-}H_{aromatic}$), 2,931 *ν*($C\text{-}H_{aliphatic}$), 1,631 *ν*($C{=}N_{thiazole}$), 1,475 *ν*(C=C), 1,111 *ν*($C\text{-}O_{phenolic}$), 756 *ν*(C–S–C). ^{1}H NMR (300 MHz, $CDCl_3$): δ = 14.03 (bs, 1H, OH), 8.31 (bs, 2H, Ar-H), 8.12 (d, J = 7.9 Hz 2H, Ar-H), 7.9 (d, J = 7.0 Hz, 2H, Ar-H), 7.56 (dt, J = 7.0 Hz, 2H, Ar-H), 7.45 (dt, J = 7.9 Hz, 2H, Ar-H), 1.50 (s, 9H, *tert*-but) ppm.

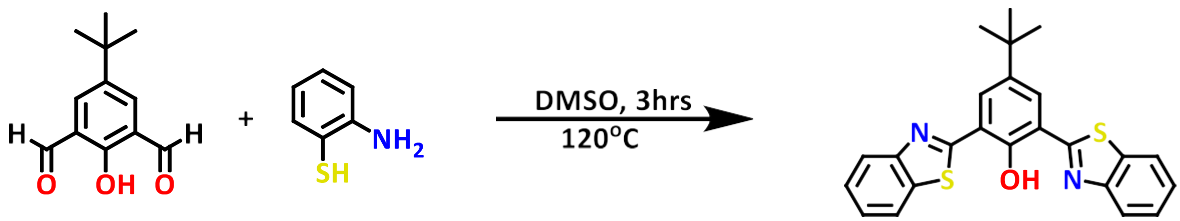

HL

Synthesis of Ni(II) complex (KRS-1)

For the synthesis of the complex, 100 mg (0.24 millimoles) of ligand (HL) was dissolved in dichloromethane and stirred at room temperature. 35μL of triethylamine was also added to it. After 10 min of stirring, 26.45 mg (0.12 millimoles) of $Ni(OAc)_2.4H_2O$ dissolved in methanol was added dropwise to the above solution in dichloromethane. The yellow precipitate obtained after stirring for about 5 hours was collected by filtration. In order to remove any impurities, it was further dissolved in N, N-dimethylformamide, and diethyl ether was added to this solution to again precipitate out the pure complex and it was again obtained by filtration and washed with diethyl ether. Yield (87%). Anal. Calcd. for Chemical Formula: $C_{54}H_{52}N_6NiO_4S_4$ (MW = 1034.2286): C, 62.61; H, 5.06; N, 8.11; S, 12.38. Found: C, 62.41; H, 5.13; N, 8.07; S,12.27.

The Ni(II) complex was characterized by FT-IR, UV-visible, MALDI-TOF MS, and X-ray crystallography.

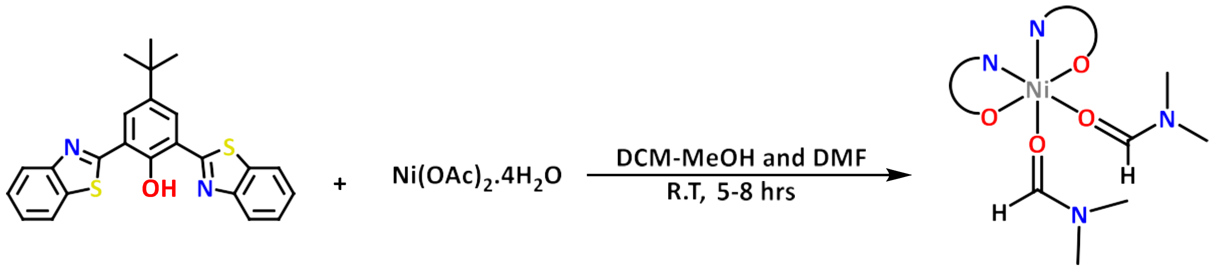

KRS-1

X-ray crystallography:

The pale-yellow crystals of the complex **KRS-1** were produced in DMF solvent using a slow evaporation process. The crystal data was collected and processed on a Bruker D8 Quest Diffractometer with a CMOS detector utilizing graphite monochromated Mo-Kα radiation (λ = 0.71073 Å) at 100 K. Crystal structures were solved using direct methods. The SHELXTL program was used to solve structure problems, refine them, and produce data.[3,4] All non-hydrogen atoms were polished anisotropically. ORTEP diagrams were generated with the MERCURY 3.10.3 software.[5]

Crystal data and structural refinement parameters for complex KRS-1:

Empirical formula	$C_{108}H_{103}N_{12}Ni_2O_8S_8$
Formula weight	2070.92
Temperature/K	100
Crystal system	triclinic
Space group	P-1
a/Å	13.4171(6)
b/Å	15.9626(8)
c/Å	26.6148(12)
α/°	89.9910(10)
β/°	89.9890(10)
γ/°	103.0520(10)
Volume/Å3	5552.9(4)
Z	2
ρ_{calc}g/cm^3	1.239
μ/mm^{-1}	0.547
F(000)	2166
Crystal size/mm^3	0.303 × 0.14 × 0.04

Radiation	MoKα (λ = 0.71073)
2Θ range for data collection/°	2.618 to 52.716
Index ranges	-16 ≤ h ≤ 16, -19 ≤ k ≤ 19, -33 ≤ l ≤ 33
Reflections collected	252512
Independent reflections	22595 [R_{int} = 0.0510, R_{sigma} = 0.0262]
Data/restraints/parameters	22595/0/1262
Goodness-of-fit on F2	1.049
Final R indexes [I>=2σ (I)]	R_1 = 0.0349, wR_2 = 0.0951
Final R indexes [all data]	R_1 = 0.0412, wR_2 = 0.0996
Largest diff. peak/hole / e Å-3	0.56/-0.40

Table 1: Summary of crystal data and data-collection parameters of complex KRS-1

Atom	Atom	Length/Å
Ni1	O1	2.0295(13)
Ni1	O2	2.0044(13)
Ni1	O3	2.0879(13)
Ni1	O4	2.1122(13)
Ni1	N2	2.0873(15)
Ni1	N3	2.0820(15)
Ni2	O5	2.0293(12)
Ni2	O6	2.0048(13)
Ni2	O7	2.0888(13)
Ni2	O8	2.1105(13)
Ni2	N7	2.0820(15)
Ni2	N8	2.0891(15)
S1	C1	1.7322(19)
S1	C7	1.7631(19)
S2	C16	1.7596(18)
S2	C17	1.7373(19)
S3	C19	1.7619(18)
S3	C20	1.7338(18)
S4	C43	1.7628(18)

Atom	Atom	Length/Å
C14	C22	1.541(3)
C14	C23	1.527(3)
C17	C18	1.399(3)
C17	C24	1.396(2)
C18	C27	1.402(3)
C19	C33	1.453(3)
C20	C21	1.407(2)
C20	C39	1.395(3)
C21	C40	1.395(3)
C24	C25	1.377(3)
C25	C26	1.398(3)
C26	C27	1.385(3)
C28	C29	1.423(3)
C28	C33	1.432(2)
C29	C30	1.388(3)
C29	C43	1.465(2)
C30	C31	1.398(2)
C31	C32	1.389(3)
C31	C46	1.533(2)

S4	C44	1.7331(19)
S5	C56	1.7350(18)
S5	C62	1.7621(19)
S6	C70	1.7320(18)
S6	C71	1.7597(17)
S7	C72	1.7595(18)
S7	C74	1.7372(19)
S8	C100	1.7642(18)
S8	C102	1.732(2)
O1	C13	1.300(2)
O2	C28	1.297(2)
O3	C34	1.238(2)
O4	C37	1.244(2)
O5	C64	1.299(2)
O6	C77	1.295(2)
O7	C83	1.235(2)
O8	C86	1.243(2)
N1	C6	1.391(2)
N1	C7	1.309(2)
N2	C16	1.312(2)
N2	C18	1.397(2)
N3	C19	1.315(2)
N3	C21	1.398(2)
N4	C37	1.324(2)
N4	C38	1.448(3)
N4	C49	1.453(3)
N5	C43	1.305(2)
N5	C45	1.385(2)
N6	C57	1.392(2)
N6	C62	1.311(2)
N7	C69	1.397(2)
N7	C71	1.318(2)
N8	C72	1.312(2)
N8	C73	1.397(2)
N9	C86	1.327(2)
N9	C87	1.448(3)
N9	C104	1.452(3)
N10	C100	1.304(2)
N10	C101	1.386(2)
N17	C34	1.315(3)
N17	C36	1.434(3)

C32	C33	1.405(3)
C39	C42	1.379(3)
C40	C41	1.381(3)
C41	C42	1.403(3)
C44	C45	1.406(3)
C44	C50	1.393(3)
C45	C53	1.398(3)
C46	C47	1.529(2)
C46	C54	1.533(3)
C46	C55	1.542(3)
C50	C51	1.376(3)
C51	C52	1.395(4)
C52	C53	1.387(3)
C56	C57	1.398(3)
C56	C61	1.399(3)
C57	C58	1.406(3)
C58	C59	1.385(3)
C59	C60	1.393(3)
C60	C61	1.384(3)
C62	C63	1.465(2)
C63	C64	1.425(2)
C63	C68	1.395(3)
C64	C65	1.434(2)
C65	C66	1.392(3)
C65	C72	1.459(2)
C66	C67	1.396(3)
C67	C68	1.391(3)
C67	C75	1.539(3)
C69	C70	1.408(2)
C69	C88	1.397(3)
C70	C91	1.397(3)
C71	C78	1.454(2)
C73	C74	1.397(2)
C73	C92	1.402(3)
C74	C95	1.399(2)
C75	C76	1.540(3)
C75	C96	1.528(3)
C75	C97	1.533(3)
C77	C78	1.432(2)
C77	C82	1.423(3)
C78	C79	1.404(2)

N17	C48	1.457(3)
N18	C83	1.315(3)
N18	C85	1.435(3)
N18	C103	1.461(3)
C1	C2	1.401(3)
C1	C6	1.397(3)
C2	C3	1.384(3)
C3	C4	1.392(3)
C4	C5	1.385(3)
C5	C6	1.404(3)
C7	C8	1.465(2)
C8	C9	1.396(3)
C8	C13	1.424(3)
C9	C10	1.393(3)
C10	C11	1.399(3)
C10	C14	1.536(3)
C11	C12	1.393(3)
C12	C13	1.432(2)
C12	C16	1.460(3)
C14	C15	1.529(3)

C79	C80	1.389(3)
C80	C81	1.398(2)
C80	C98	1.532(2)
C81	C82	1.388(3)
C82	C100	1.464(2)
C88	C89	1.384(3)
C89	C90	1.402(3)
C90	C91	1.382(3)
C92	C93	1.383(2)
C93	C94	1.395(3)
C94	C95	1.381(3)
C98	C99	1.531(2)
C98	C105	1.540(3)
C98	C106	1.537(3)
C101	C102	1.408(3)
C101	C107	1.400(3)
C102	C110	1.396(3)
C107	C108	1.382(3)
C108	C109	1.395(4)
C109	C110	1.377(3)

Table 2: Bond Lengths for complex KRS-1.

Atom	Atom	Atom	Angle/˚
O1	Ni1	O3	90.51(5)
O1	Ni1	O4	176.94(5)
O1	Ni1	N2	84.61(5)
O1	Ni1	N3	89.88(5)
O2	Ni1	O1	95.67(5)
O2	Ni1	O3	171.97(5)
O2	Ni1	O4	87.21(5)
O2	Ni1	N2	88.53(6)
O2	Ni1	N3	85.64(5)
O3	Ni1	O4	86.53(5)
N2	Ni1	O3	86.94(6)
N2	Ni1	O4	94.45(5)
N3	Ni1	O3	99.54(5)
N3	Ni1	O4	91.38(5)

Atom	Atom	Atom	Angle/˚
C29	C28	C33	116.81(16)
C28	C29	C43	120.49(16)
C30	C29	C28	120.63(16)
C30	C29	C43	118.88(16)
C29	C30	C31	122.60(17)
C30	C31	C46	119.12(16)
C32	C31	C30	117.02(16)
C32	C31	C46	123.86(16)
C31	C32	C33	122.52(16)
C28	C33	C19	119.27(16)
C32	C33	C19	120.62(16)
C32	C33	C28	119.90(16)
O3	C34	N17	124.5(2)
O4	C37	N4	124.60(18)

N3	Ni1	N2	171.55(6)
O5	Ni2	O7	90.49(5)
O5	Ni2	O8	176.91(5)
O5	Ni2	N7	89.93(5)
O5	Ni2	N8	84.58(5)
O6	Ni2	O5	95.60(5)
O6	Ni2	O7	172.04(5)
O6	Ni2	O8	87.29(5)
O6	Ni2	N7	85.63(5)
O6	Ni2	N8	88.52(6)
O7	Ni2	O8	86.53(5)
O7	Ni2	N8	86.95(6)
N7	Ni2	O7	99.53(5)
N7	Ni2	O8	91.39(5)
N7	Ni2	N8	171.56(6)
N8	Ni2	O8	94.41(5)
C1	S1	C7	89.09(9)
C17	S2	C16	89.54(9)
C20	S3	C19	90.05(9)
C44	S4	C43	88.77(9)
C56	S5	C62	89.21(9)
C70	S6	C71	90.08(8)
C74	S7	C72	89.50(9)
C102	S8	C100	88.92(9)
C13	O1	Ni1	117.83(11)
C28	O2	Ni1	124.21(11)
C34	O3	Ni1	120.91(13)
C37	O4	Ni1	119.72(12)
C64	O5	Ni2	117.95(11)
C77	O6	Ni2	124.27(11)
C83	O7	Ni2	120.92(13)
C86	O8	Ni2	119.73(12)
C7	N1	C6	111.10(16)
C16	N2	Ni1	119.75(12)
C16	N2	C18	111.91(15)
C18	N2	Ni1	127.03(12)
C19	N3	Ni1	120.95(12)
C19	N3	C21	111.93(15)
C21	N3	Ni1	127.11(12)
C37	N4	C38	121.34(17)
C37	N4	C49	120.94(18)

C42	C39	C20	117.89(17)
C41	C40	C21	118.72(17)
C40	C41	C42	120.88(17)
C39	C42	C41	121.29(17)
N5	C43	S4	115.53(14)
N5	C43	C29	122.63(17)
C29	C43	S4	121.81(14)
C45	C44	S4	109.72(14)
C50	C44	S4	128.59(17)
C50	C44	C45	121.69(19)
N5	C45	C44	115.09(17)
N5	C45	C53	125.48(19)
C53	C45	C44	119.42(18)
C31	C46	C54	109.99(15)
C31	C46	C55	108.69(15)
C47	C46	C31	111.82(15)
C47	C46	C54	107.87(15)
C47	C46	C55	108.73(15)
C54	C46	C55	109.72(16)
C51	C50	C44	117.9(2)
C50	C51	C52	121.4(2)
C53	C52	C51	121.0(2)
C52	C53	C45	118.7(2)
C57	C56	S5	109.68(14)
C57	C56	C61	121.71(18)
C61	C56	S5	128.60(16)
N6	C57	C56	115.21(16)
N6	C57	C58	125.41(19)
C56	C57	C58	119.38(18)
C59	C58	C57	118.6(2)
C58	C59	C60	121.52(18)
C61	C60	C59	120.71(19)
C60	C61	C56	118.1(2)
N6	C62	S5	114.97(14)
N6	C62	C63	123.76(17)
C63	C62	S5	121.26(14)
C64	C63	C62	119.45(17)
C68	C63	C62	119.60(16)
C68	C63	C64	120.88(16)
O5	C64	C63	120.48(16)
O5	C64	C65	122.66(16)

C38	N4	C49	117.56(18)
C43	N5	C45	110.83(16)
C62	N6	C57	110.93(16)
C69	N7	Ni2	127.17(11)
C71	N7	Ni2	120.98(12)
C71	N7	C69	111.84(15)
C72	N8	Ni2	119.70(12)
C72	N8	C73	112.05(15)
C73	N8	Ni2	126.93(12)
C86	N9	C87	121.41(18)
C86	N9	C104	120.96(18)
C87	N9	C104	117.47(18)
C100	N10	C101	110.90(16)
C34	N17	C36	120.8(2)
C34	N17	C48	122.1(2)
C36	N17	C48	117.1(2)
C83	N18	C85	120.8(2)
C83	N18	C103	122.3(2)
C85	N18	C103	116.9(2)
C2	C1	S1	128.54(17)
C6	C1	S1	109.94(14)
C6	C1	C2	121.51(18)
C3	C2	C1	118.1(2)
C2	C3	C4	120.78(19)
C5	C4	C3	121.42(19)
C4	C5	C6	118.6(2)
N1	C6	C1	114.96(16)
N1	C6	C5	125.47(19)
C1	C6	C5	119.58(18)
N1	C7	S1	114.91(14)
N1	C7	C8	123.91(17)
C8	C7	S1	121.17(14)
C9	C8	C7	119.60(16)
C9	C8	C13	120.74(16)
C13	C8	C7	119.57(17)
C10	C9	C8	122.53(17)
C9	C10	C11	116.61(17)
C9	C10	C14	124.37(17)
C11	C10	C14	119.00(16)
C12	C11	C10	123.29(17)
C11	C12	C13	119.82(17)

C63	C64	C65	116.86(17)
C64	C65	C72	120.50(17)
C66	C65	C64	119.76(16)
C66	C65	C72	119.72(16)
C65	C66	C67	123.20(17)
C66	C67	C75	118.82(16)
C68	C67	C66	116.97(17)
C68	C67	C75	124.19(17)
C67	C68	C63	122.27(17)
N7	C69	C70	114.43(15)
C88	C69	N7	125.43(16)
C88	C69	C70	120.07(16)
C69	C70	S6	109.60(13)
C91	C70	S6	129.05(14)
C91	C70	C69	121.24(17)
N7	C71	S6	114.03(13)
N7	C71	C78	127.31(16)
C78	C71	S6	118.42(13)
N8	C72	S7	114.18(13)
N8	C72	C65	126.12(16)
C65	C72	S7	119.69(14)
N8	C73	C92	126.17(16)
C74	C73	N8	114.14(16)
C74	C73	C92	119.68(16)
C73	C74	S7	110.05(13)
C73	C74	C95	121.63(18)
C95	C74	S7	128.29(15)
C67	C75	C76	108.52(16)
C96	C75	C67	110.12(17)
C96	C75	C76	109.35(18)
C96	C75	C97	108.75(17)
C97	C75	C67	111.88(16)
C97	C75	C76	108.18(17)
O6	C77	C78	123.36(16)
O6	C77	C82	119.89(15)
C82	C77	C78	116.72(16)
C77	C78	C71	119.19(16)
C79	C78	C71	120.54(15)
C79	C78	C77	120.06(16)
C80	C79	C78	122.43(16)
C79	C80	C81	117.03(16)

C11	C12	C16	119.62(16)
C13	C12	C16	120.55(17)
O1	C13	C8	120.33(16)
O1	C13	C12	122.72(16)
C8	C13	C12	116.95(16)
C10	C14	C22	108.43(16)
C15	C14	C10	111.89(16)
C15	C14	C22	108.29(17)
C23	C14	C10	110.08(17)
C23	C14	C15	108.70(17)
C23	C14	C22	109.41(18)
N2	C16	S2	114.26(13)
N2	C16	C12	126.01(16)
C12	C16	S2	119.72(14)
C18	C17	S2	109.91(13)
C24	C17	S2	128.49(15)
C24	C17	C18	121.57(18)
N2	C18	C17	114.30(16)
N2	C18	C27	125.98(16)
C17	C18	C27	119.72(16)
N3	C19	S3	113.98(13)
N3	C19	C33	127.41(16)
C33	C19	S3	118.36(13)
C21	C20	S3	109.56(13)
C39	C20	S3	129.03(14)
C39	C20	C21	121.30(17)
N3	C21	C20	114.47(16)
C40	C21	N3	125.55(16)
C40	C21	C20	119.91(16)
C25	C24	C17	118.23(17)
C24	C25	C26	120.65(17)
C27	C26	C25	121.56(19)
C26	C27	C18	118.23(17)
O2	C28	C29	119.93(16)
O2	C28	C33	123.22(16)

C79	C80	C98	123.77(15)
C81	C80	C98	119.19(16)
C82	C81	C80	122.67(17)
C77	C82	C100	120.45(16)
C81	C82	C77	120.59(16)
C81	C82	C100	118.94(16)
O7	C83	N18	124.6(2)
O8	C86	N9	124.60(18)
C89	C88	C69	118.53(17)
C88	C89	C90	120.97(17)
C91	C90	C89	121.31(17)
C90	C91	C70	117.86(17)
C93	C92	C73	118.25(18)
C92	C93	C94	121.77(18)
C95	C94	C93	120.56(17)
C94	C95	C74	118.06(17)
C80	C98	C105	108.76(14)
C80	C98	C106	109.93(15)
C99	C98	C80	111.80(15)
C99	C98	C105	109.00(15)
C99	C98	C106	107.87(15)
C106	C98	C105	109.45(16)
N10	C100	S8	115.41(13)
N10	C100	C82	122.68(16)
C82	C100	S8	121.88(14)
N10	C101	C102	115.10(17)
N10	C101	C107	125.50(19)
C107	C101	C102	119.40(18)
C101	C102	S8	109.62(14)
C110	C102	S8	128.72(17)
C110	C102	C101	121.66(19)
C108	C107	C101	118.6(2)
C107	C108	C109	121.3(2)
C110	C109	C108	121.32(19)
C109	C110	C102	117.8(2)

Table 3: Bond Angles for complex KRS-1.

Preparation of $PrP_{106\text{-}126}$ fibrils:

The $PrP_{106\text{-}126}$ fibrillar aggregates were prepared as per earlier reports.[6] Frozen $PrP_{106\text{-}126}$ peptides were dissolved in 500 µL of 1,1,1,3,3,3-hexafluoro-2-propanol (HFIP) to disrupt any trace of preformed aggregates. The peptide solution was kept overnight, peptide aliquots were prepared, and HFIP was evaporated by passing N_2 gas and $PrP_{106\text{-}126}$ peptide stored at −80 °C. The final stock solutions of $PrP_{106\text{-}126}$ (monomeric) were prepared by dissolving peptides in molecular grade DMSO at a final conc. of 1 mM. The ThT-fluorescence assay was used to observe the formation of $PrP_{106\text{-}126}$ soluble aggregates. The 100 µM of final peptide concentrations were made by diluting the 1 mM stock solution of $PrP_{106\text{-}126}$ peptide in 10 mM phosphate buffer (pH 7.4), incubated at 37 °C for 24 h in a 96-well microtiter plate (200 µL total volume).

Job's Plot Analysis:[7]

$PrP_{106\text{-}126}$ fibrils were prepared as described earlier. These $PrP_{106\text{-}126}$ fibrils were then diluted to a final concentration of 10, 20, 30, 40, 50, 60, 70, 80, 90, and 100 µM. Photoluminescence was observed by varying the **KRS−1** and peptide ratio with fixed total concentration (**KRS-1** + $PrP_{106\text{-}126}$ fibrils) of 100 µM. The molar ratio of **KRS-1** is defined as the moles of **KRS-1** divided by the total moles in the solution, that is, **KRS-1** + $PrP_{106\text{-}126}$ fibrils.

Benesi-Hildebrand Plot:[8]

By UV-visible: Binding constant (K) between Ni^{2+} and ligand (HL) was calculated according to the Benesi-Hildebrand equation as stated below.

$$log\frac{A - A_{min}}{A_{max} - A} = logK + nlog[Ni^{2+}]$$

Where, A = absorbance intensity of ligand (HL) obtained with Ni^{2+} ions; A_{min} = absorbance intensity of ligand (HL) only; A_{max} = absorbance intensity of ligand (HL) in the presence of Ni^{2+} ions, the stoichiometry (n) was found to be 0.57 and the binding constant (*K*) was found to be 1.79 × 10^{12} M^{-2}.

By fluorescence: The binding constant value between KRS-1 and $PrP_{106\text{-}126}$ was calculated using the Benesi–Hildebrand equation as stated below.

$$\frac{1}{F - F_o} = \frac{1}{K^{0.5}(F_{max} - F_o)[Ni^{2+}]^{0.5}} + \frac{1}{F_{max} - F_o}$$

Where, F = emission intensity at a particular concentration of KRS-1; F_o = emission intensity of PrP only; F_{max} = maximum emission intensity observed in the presence of KRS-1. The binding constant (*K*) was found to be 2.05 × 10^6 M^{-2}.

Evan's Method:[9,10]

A 500 µL solution of **KRS-1** containing HMDS (internal standard) in DMSO-d_6 was taken in a

Wilmad screw-cap NMR tube. HMDS in DMSO-d_6 was taken in Wilmad coaxial insert stem, and the tube was carefully inserted inside the screw-cap NMR tube. ^{1}H NMR spectra of **KRS-1** was recorded in a Bruker 500 MHz NMR instrument at 25 °C. Paramagnetic susceptibility of the **KRS-1** was determined using the following equation: $\chi_P = \chi_0 + 3000\Delta\nu/4\pi\nu_0 cM$ Here, χ_0 = diamagnetic susceptibility, $\Delta\nu$ = shift of frequency of the methyl protons of HMDS in Hz, ν_0 = frequency of the NMR instrument used during the measurement, c = concentration of the **KRS-1**, and M = molecular weight. Effective magnetic moment (μ_{eff}) of the **KRS-1** was determined using the following equation: $\mu_{eff} = (3k_B\chi_P T/NA\beta^2)^{1/2} = (8 \times \chi_P \times T)^{1/2}$ Where k_B = Boltzmann's constant, T = Temperature, N_A = Avogadro's number, β = Bohr magneton. The ratio of $3k_B / N_A\beta^2 \approx 8$. Molar paramagnetic susceptibility was estimated from the χ_P value and molecular weight of the **KRS-1**.

Detection of $PrP_{106\text{-}126}$ aggregates in neuronal HT-22 cells:

Cell culture and treatments

HT-22 cells were cultured in Dulbecco's Modified Eagle Medium (DMEM) medium and were maintained at 37°C in an incubator, supplied with 5% CO_2. After 24 hours of incubation, the cells were trypsinized and were seeded in multi-well plates. At 60% confluency, the cells were treated with fibrillar $PrP_{106\text{-}126}$ with the probe (KRS-1) and proceeded according to the respective experiments.

MTT assay for cell viability

The cytotoxicity of the probe **KRS-1** was assessed according to the previously published protocol[11]. 5 × 10^3 HT-22 cells were seeded in a 96-well plate, which was then incubated with test compounds for 24 hours. Thereafter, 10 µL MTT (stock conc. 5mg/mL) was added to each well. After 4 hours of incubation, the formazan particles were dissolved in DMSO. The optical density of the solubilized, purple-colored formazan crystals was measured at 570 nm in ELSIA plate reader (Fluostar optima, BMG Labtech, Germany). The percentage inhibition was calculated as follows:

$$\text{[illegible] y} = \frac{\text{[illegible]}}{\text{mean absorbance of vehicle treated cells}} \times 100$$

All data was obtained by performing three independent experiments.

Molecular docking

Using the LANL2DZ basis set and the B3LYP level of theory, molecular structure optimization and frequency calculation of the complex were performed.[12] The Gaussian 16 software suite was used to perform the calculations.[13] Using the Autodock 4.2 program, molecular docking studies were carried out to investigate the interaction between the **KRS-1** and the fibrillar prion protein.[14] Since there is no PDB code for a prion protein having peptide sequence 106–126, the protein structure of the prion fibrils with PDB code 6UUR (fibrils consisting of the sequence from 94 to 178) was used, and the structure was selected from the RCSB Protein Data Bank (PDB).[15] For molecular docking, the PDBQT files of the ligand and protein were created using Autodock tools (ADT).[14] The protein binding sites and peptide sequences ranging from 106 to 126 were determined, and the molecular docking grid was created as per this information. The grid center was specified at 217.575 x 226.252 x 135.291 xyz-coordinates, respectively. For docking, we used the Lamarckian genetic algorithm (LGA) and up to 2 500 000 energy evaluations. The protein–ligand complex's docking positions and 2-D interaction plots were visualized using the Discovery Studio 9 program.

MALDI-TOF MS

The peptide sample utilized in the MALDI-TOF MS experiments was maintained at a constant concentration of 100 µM. The peptide was incubated for 24 hours for fibrils formation. The probe **KRS-1** was added in an amount half to that of the aggregated $PrP_{106–126}$ sample. Prior to the experiment, the sample was incubated for 30 minutes. The 2,5-dihyrdoxy benzoic acid (DHB) matrix and sample were separately dissolved in TA50 solution (ACN: 0.1% TFA–H2O, V/V = 50/50). A manual aliquot of 1 µL of the sample matrix solution ($V_{peptide}/V_{matrix}$ = 50/50) was spotted onto the Bruker Daltonics stainless steel target plate. The sample was examined using an Ultraflextreme MALDI-TOF MS (Bruker Daltonics, Germany) after the droplet had been air-dried at ambient temperature. Each mass spectrum was acquired within a mass-to-charge ratio (m/z) range of 0–2600 in the reflectron positive mode.

The Quantum Yield of KRS-1

$[Ru(bpy)_3]^{2+}$, which has a known quantum yield of **0.064** in acetonitrile solution at room temperature, was employed as a reference to determine the quantum yield of **KRS-1**. The **KRS-1** and $[Ru(bpy)_3](PF_6)_2$ solutions were prepared in acetonitrile with UV–Vis absorption peaks that were maintained at or below 0.1. The absorption and PL spectra were recorded at an excitation wavelength of 430 nm, and the fluorescence peak areas were measured using photoluminescence (PL) spectra. The quantum yield was determined by employing the subsequent formula:

$$QY = QYs \times \frac{I}{Is} \times \frac{As}{A} \times \frac{\eta 2}{\eta s 2} \times 100\%$$

1. QY is the quantum yield of the **KRS-1**.
2. QYs is the quantum yield of the reference i.e., $[Ru(bpy)_3](PF_6)_2$.
3. *I* and *Is* are the integral areas of the fluorescence peaks for the **KRS-1** and the reference, respectively.
4. *A* and *As* are the absorbance values for **KRS-1** and the reference, respectively.
5. η are the refractive indices of the solvents.

Supplementary Figures

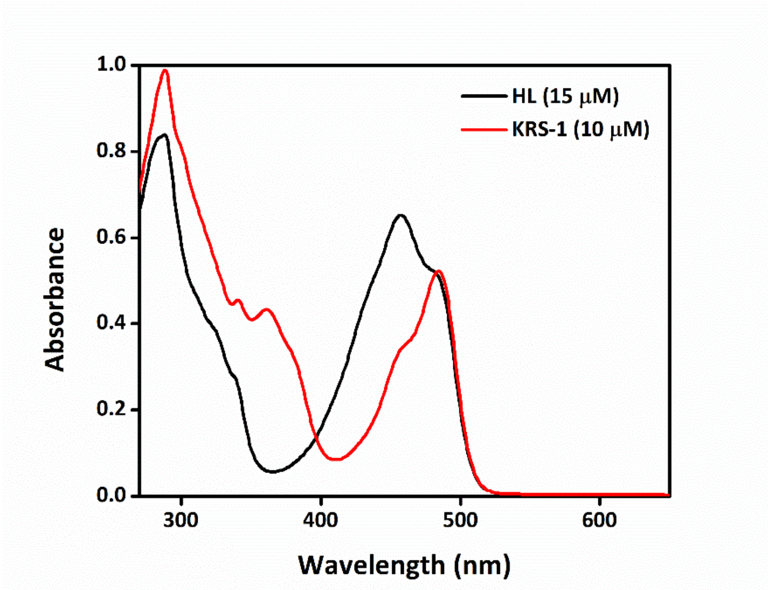

Figure S1: UV-Visible Absorption Spectra in DMSO (Biological Grade).

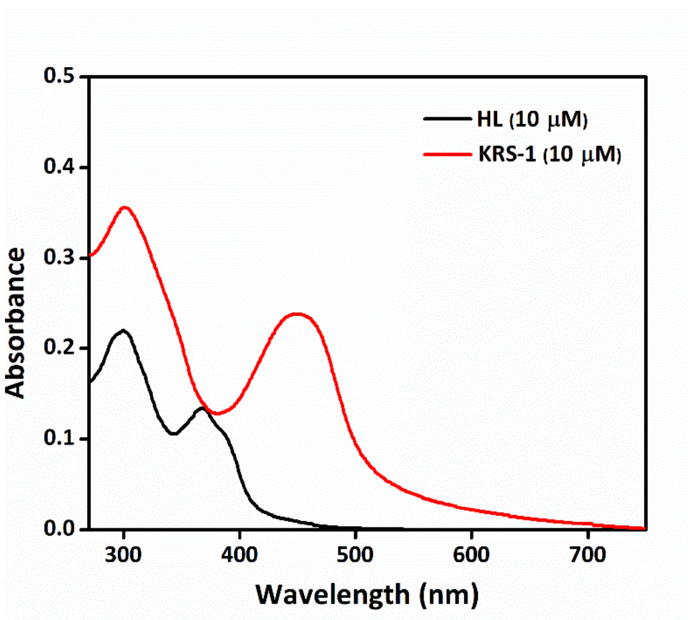

Figure S2: UV-Visible Absorption Spectra in PBS buffer at pH 7.4 using stock solutions prepared in biological grade DMSO.

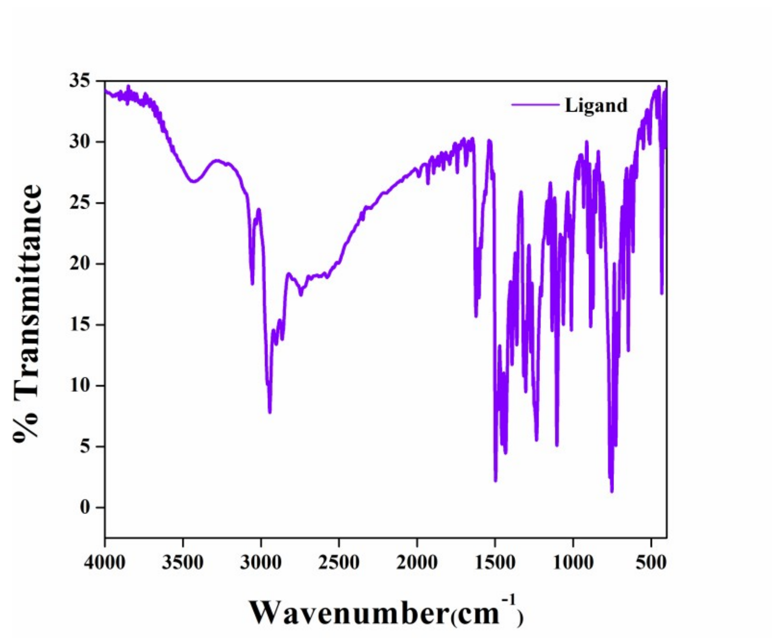

Figure S3: FT-IR Spectra of Ligand (HL).

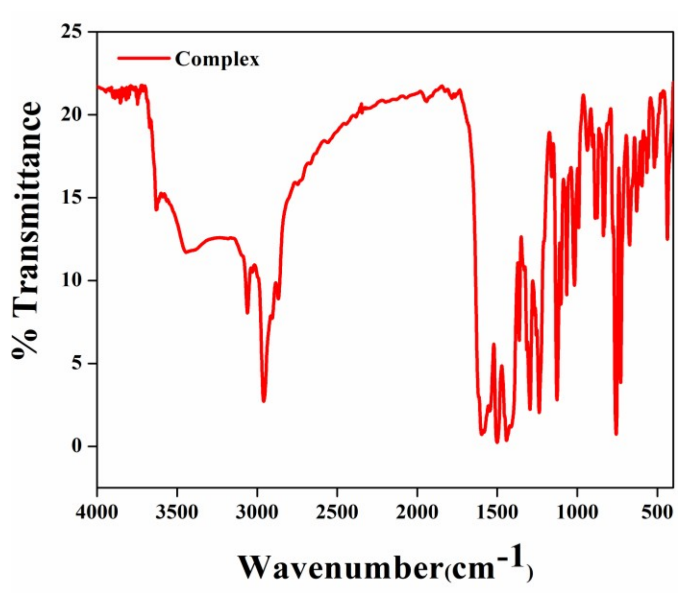

Figure S4: FT-IR Spectra of complex (**KRS-1**).

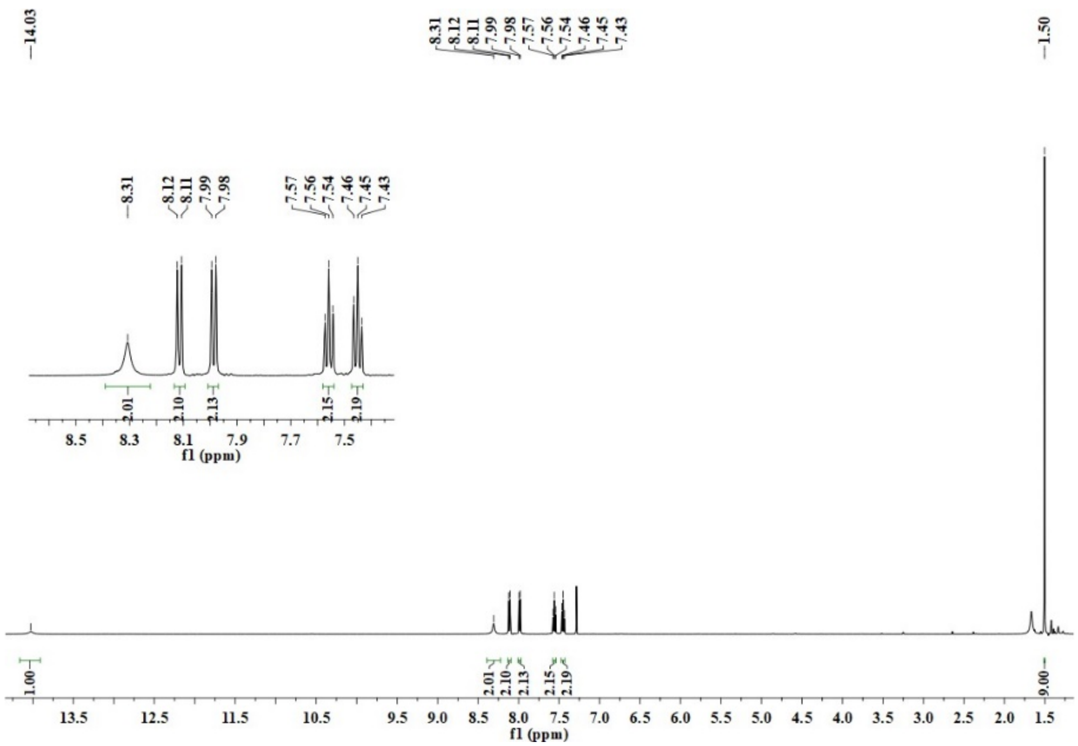

Figure S5: ^1H NMR spectra of bis-benzothiazole Ligand (HL) in $CDCl_3$.

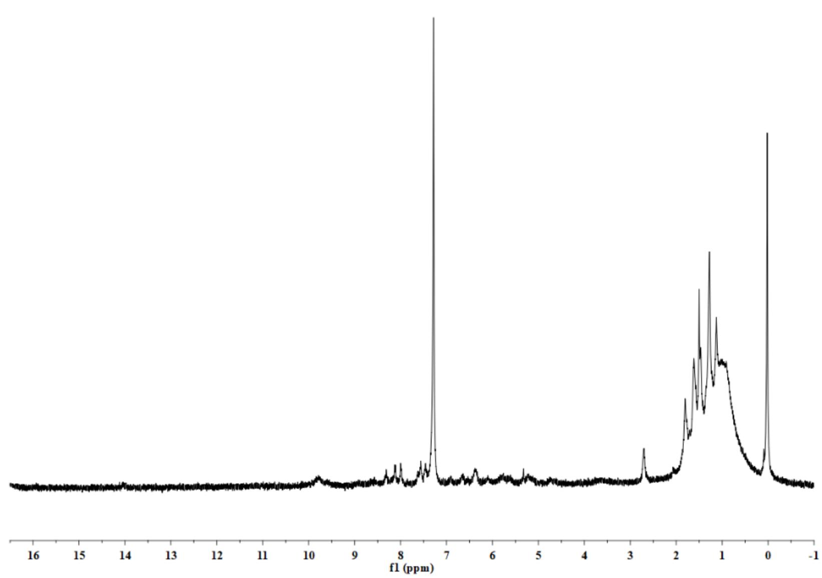

Figure S6: ^1H NMR spectra of **KRS-1** in $CDCl_3$.

(a)

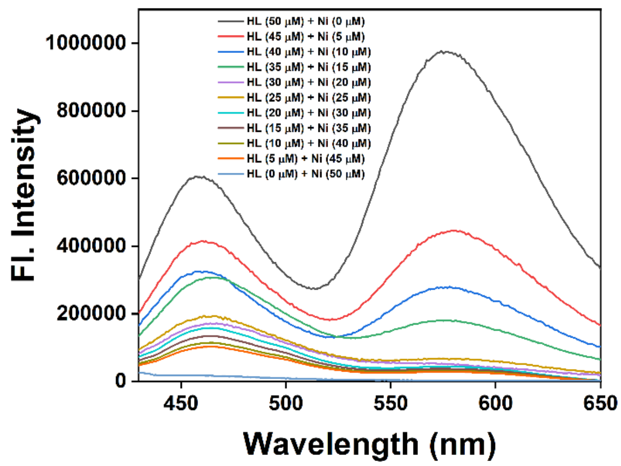

(b)

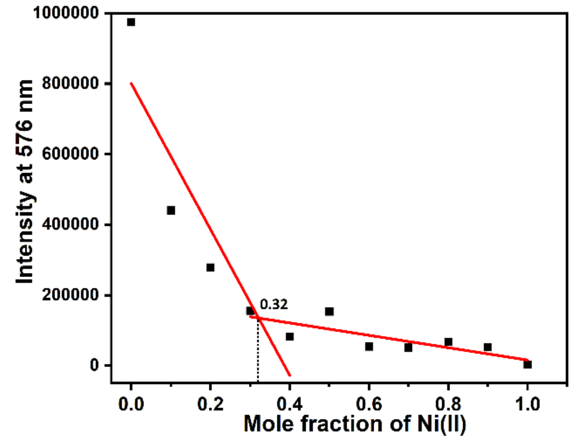

(c)

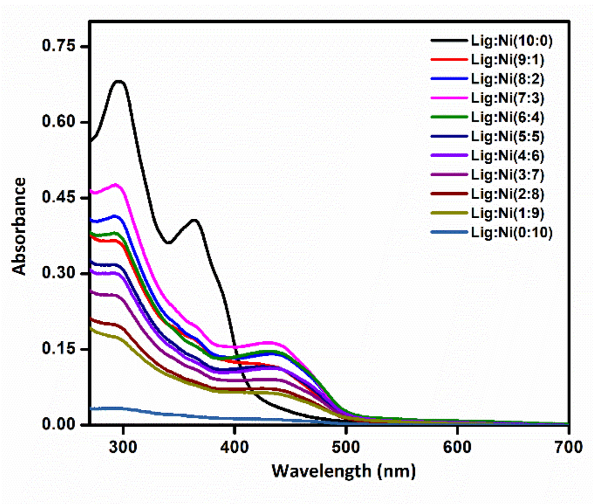

(d)

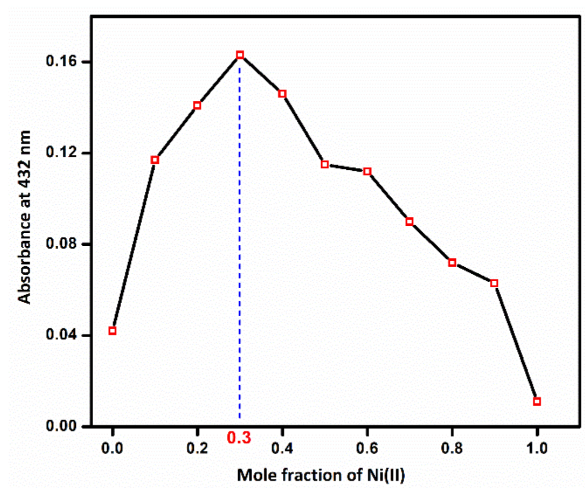

Figure S7: (a) Fluorescence titration between HL and Ni(II) in PBS buffer at pH = 7.4 by keeping the total concentration of HL and Ni(II) constant at 50 μM (λ_{ex}= 360 nm). **(b)** Job's plot analysis of the photoluminescence of **HL** in the presence of Ni(II) ions. The mole fraction of the Ni(II) and Ligand (HL) was varied, while the total concentration of the two components was kept constant at 50 μM. The stoichiometry of binding between HL and Ni(II) was found to be **2:1**, corresponding to the mole fraction of Ni(II) **0.32** calculated using the intercept of two slopes.[16] **(c)** UV-visible titration between HL and Ni(II) in PBS buffer at pH = 7.4 by keeping the total concentration of HL and Ni(II) constant at 50 μM. **(d)** The stoichiometry of binding between HL and Ni(II) was found to be **2:1**, corresponding to the mole fraction of Ni(II) 0.3 calculated by plotting the graph between the absorbance value at 432 nm and mole fraction of Ni(II).

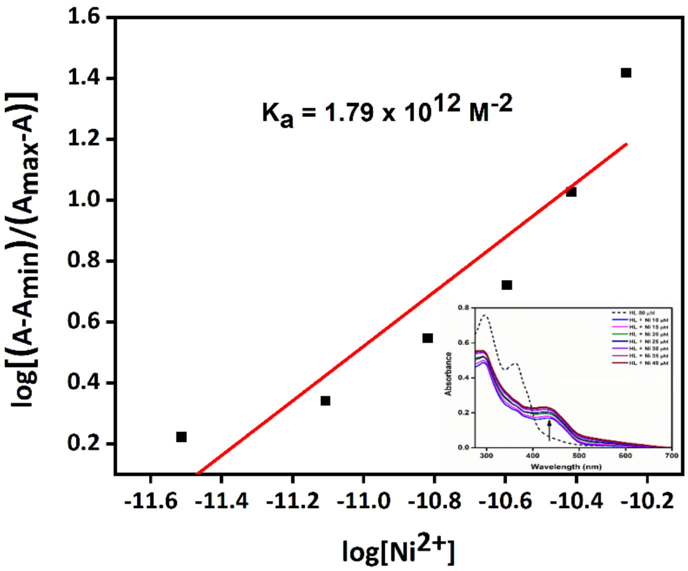

Figure S8: Determination of binding constant (K_a) by Benesi–Hildebrand equation from UV-vis titration data of ligand (50 µM) with varying Ni^{2+} concentration in PBS buffer pH 7.4 at wavelength 432 nm (**inset**- UV visible titration spectra).

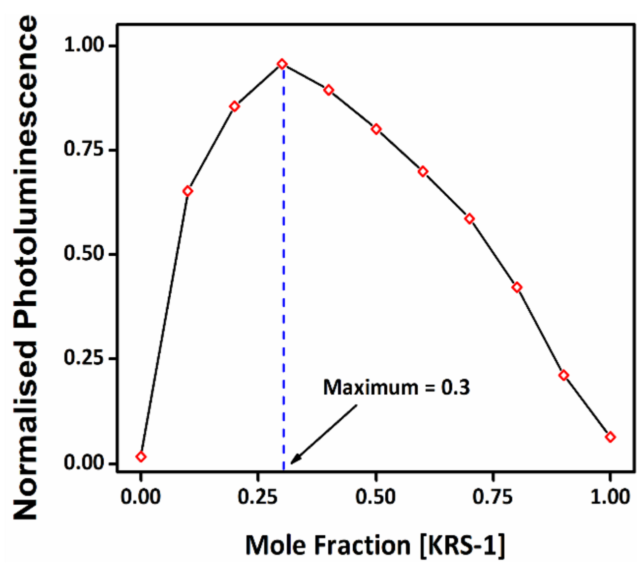

Figure S9: Job's plot analysis of the photoluminescence of **KRS-1** in the presence of fibrillar $PrP_{106-126}$ aggregates. The mole fraction of the **KRS-1** and fibrillar $PrP_{106-126}$ aggregates was varied, while the total concentration of the two components was kept constant at 100 µM.

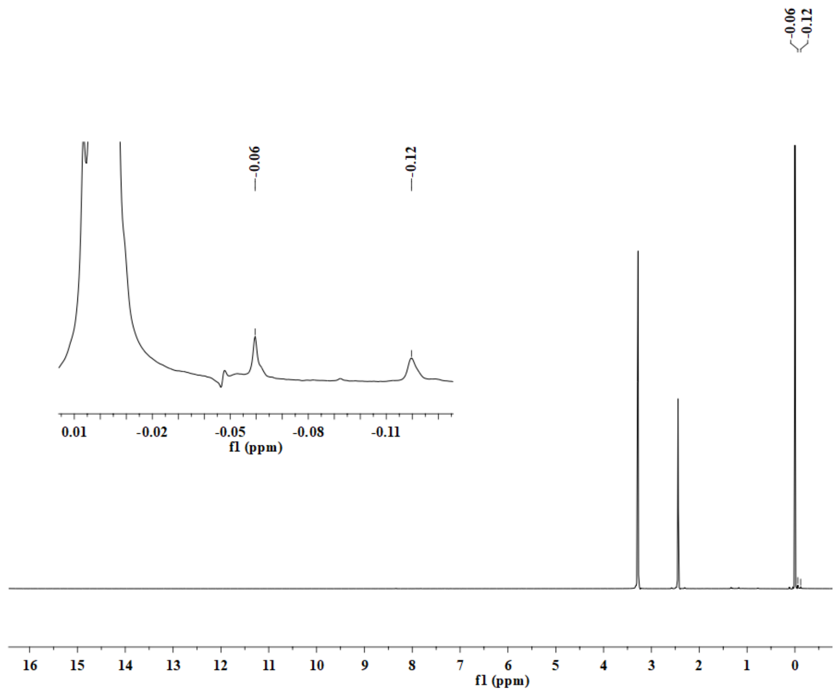

Figure S10: The shift of methyl protons of HMDS was observed (0.06 ppm) for **KRS-1** (6.15×10^{-3} M) in DMSO-d_6 at 25 °C. This shift value provides a magnetic moment value (μ_{eff}) of 2.61 BM.

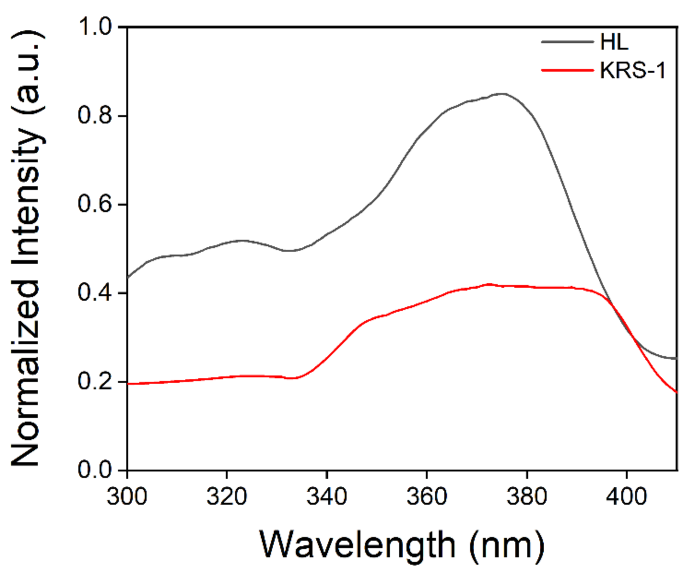

Figure S11: Excitation spectra of HL and **KRS-1**. λ_{em} = 576 nm.

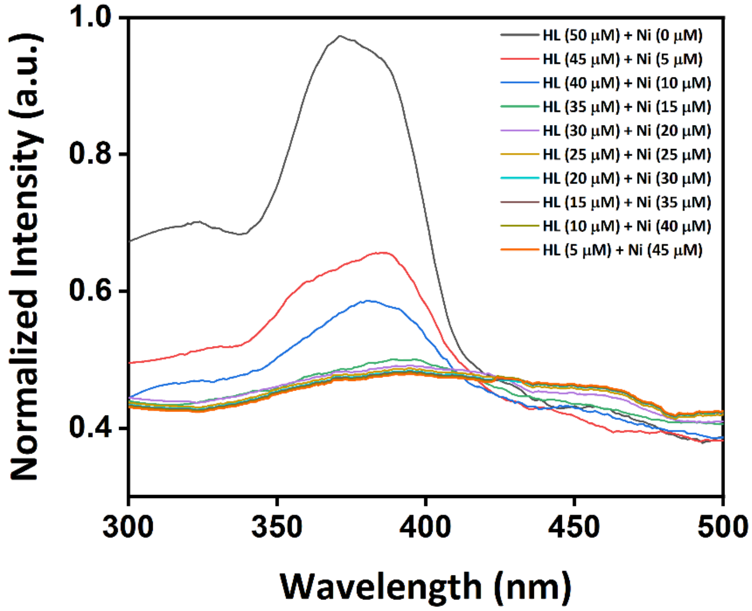

Figure S12: Change in excitation spectra of ligand (HL) upon addition of Ni(II) in PBS buffer of pH = 7.4. λ_{em} = 576 nm.

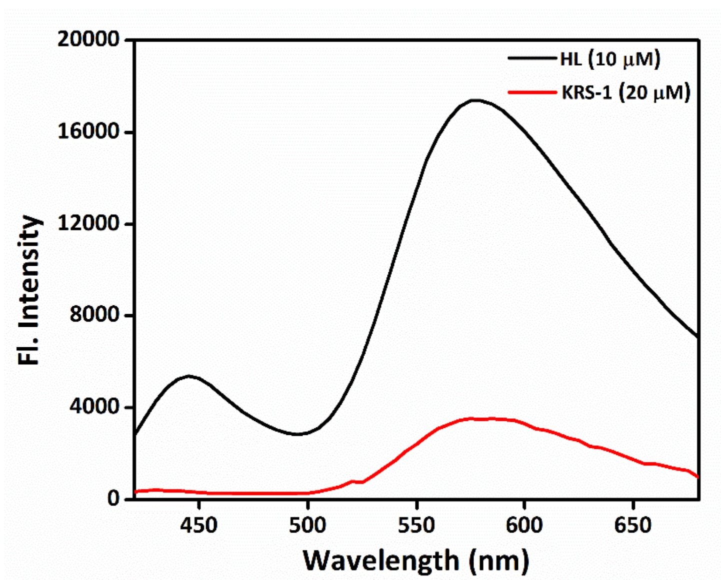

Figure S13: Emission spectra of HL and **KRS-1** in PBS at pH **= 7.4.** λ_{ex} = 360 nm.

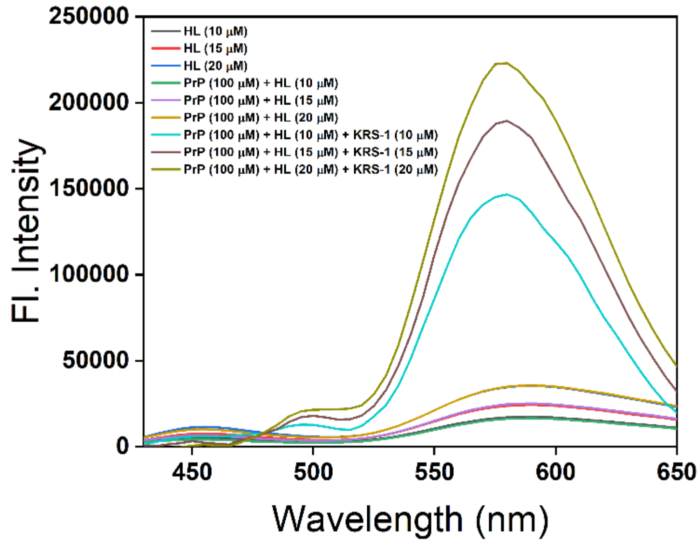

Figure S14: **KRS-1** behavior in the presence of Ligand (HL) on treatment with fibrillar $PrP_{106\text{-}126}$ aggregates in PBS at pH **= 7.4.** λ_{ex} = 360 nm.

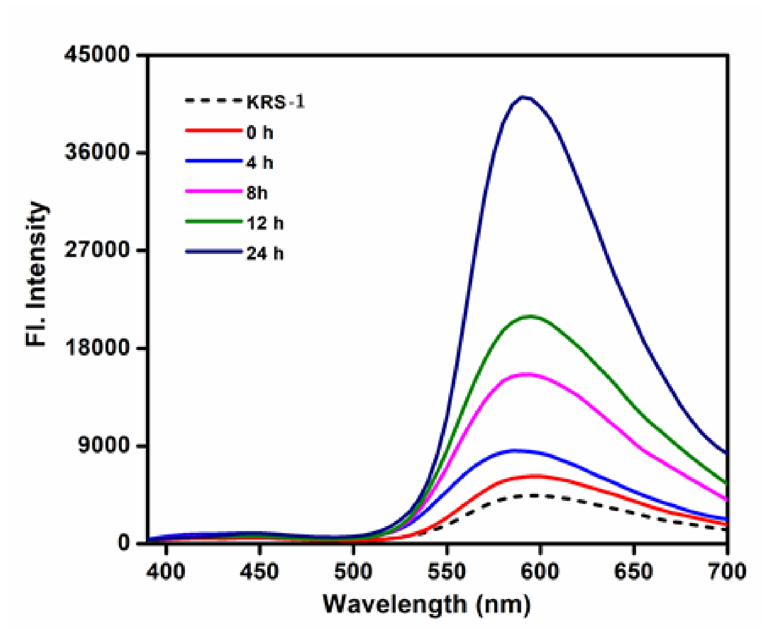

Figure S15: $PrP_{106\text{-}126}$ samples were incubated for various time intervals in the absence of **KRS-1**, ranging from 0, 4, 8, 12, and 24 hours in PBS at pH = 7.4. λ_{ex} = 360 nm. These samples were then treated immediately with **KRS-1**, and fluorescence intensity was measured.

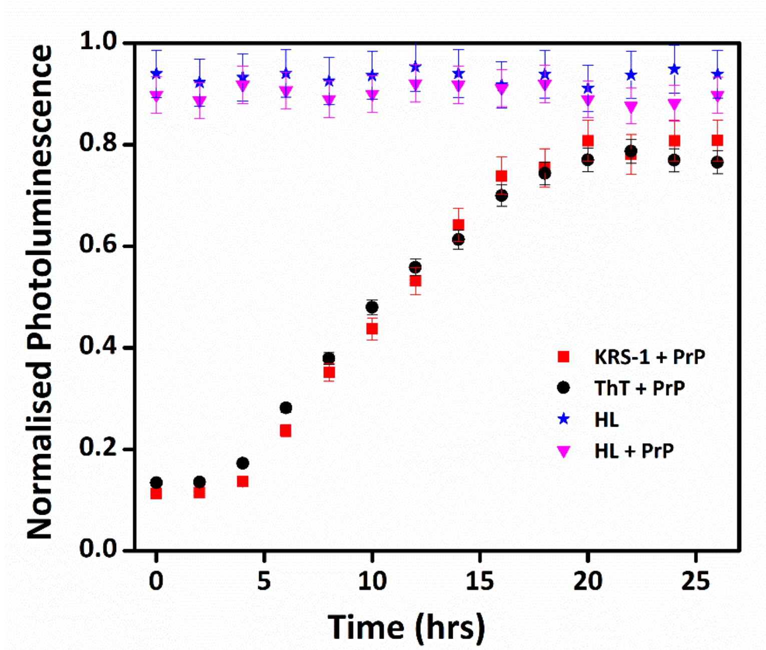

Figure S16: Control time-dependent studies of HL and **KRS-1** using ThT as a standard

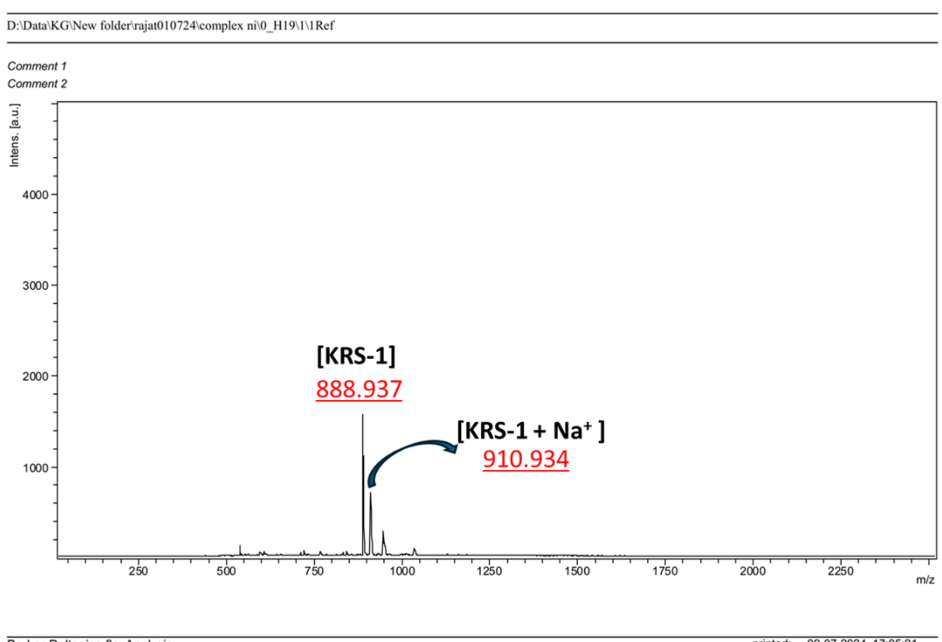

Figure S17: MALDI-TOF MS spectrum of **KRS-1**.

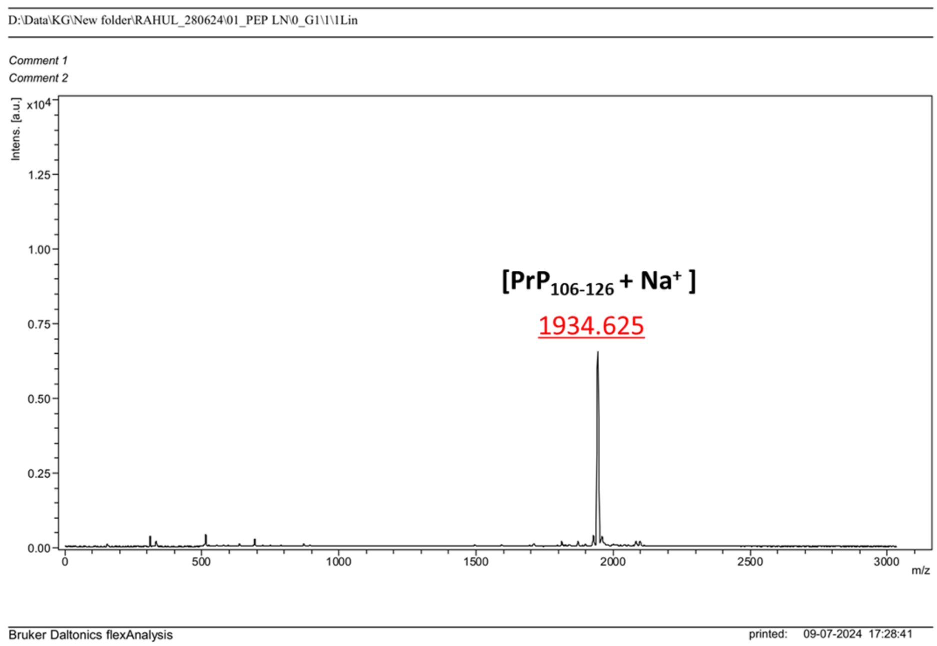

Figure S18: MALDI-TOF MS spectrum of native $PrP_{106-126}$ peptide.

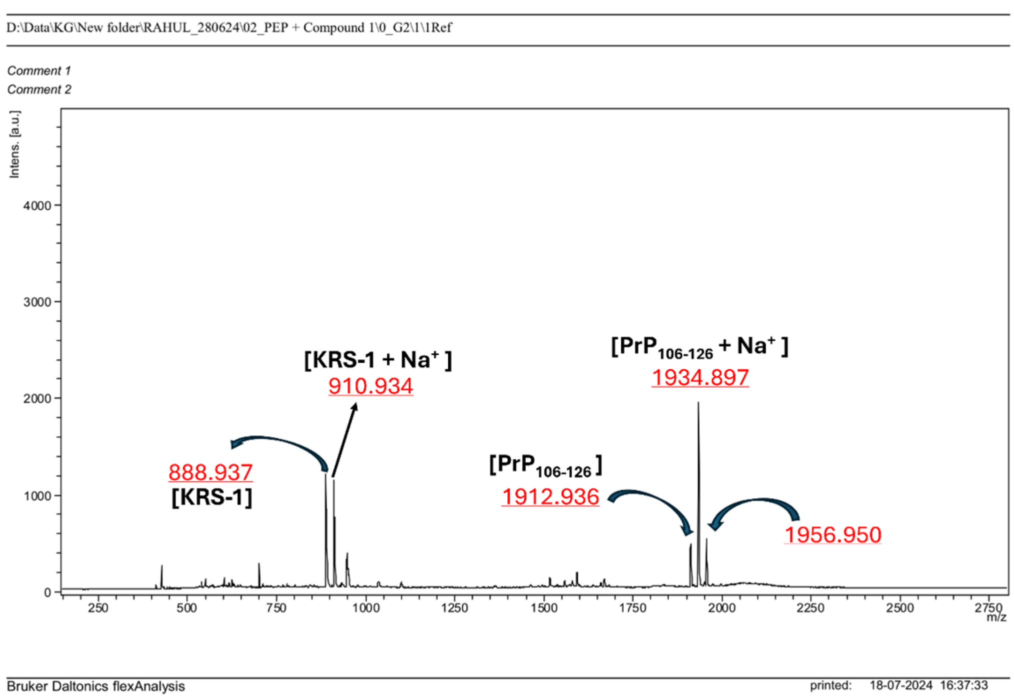

Figure S19: MALDI-TOF MS spectrum of **KRS-1** along with aggregated $PrP_{106-126}$ peptide (first peptide was incubated at 37 ^{o}C for 24 hrs. and then **KRS-1** was added, and the spectrum was recorded)

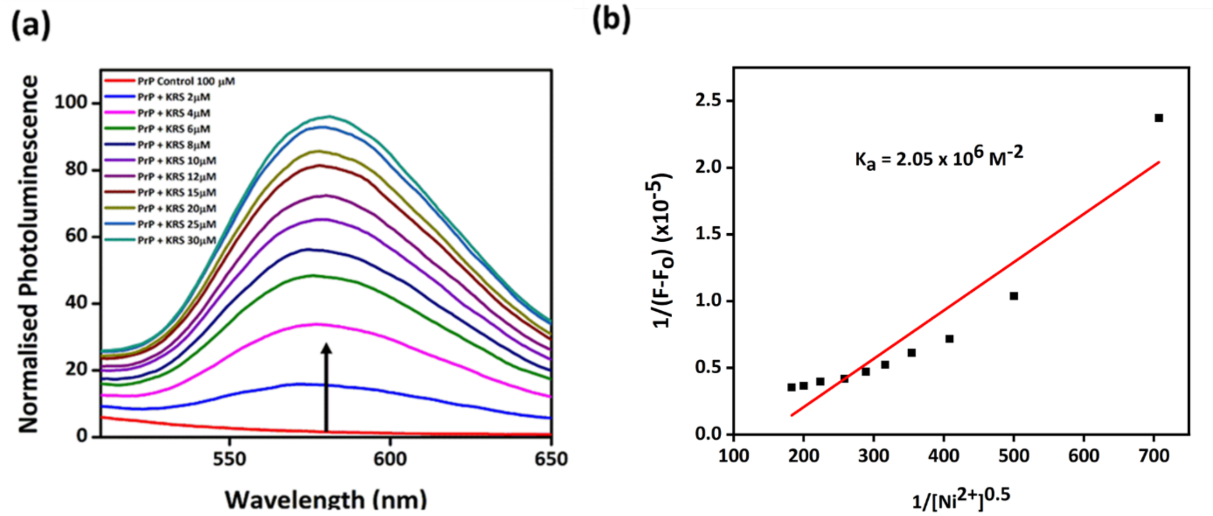

Figure S20: **(a)** Fluorescence titration curve for **KRS-1** by keeping the concentration of $PrP_{106\text{-}126}$ fibrils constant at 100 μM. **(b)** Fitting of this data to the Benesi- Hildebrand equation for calculating the binding constant (K_a) revealed a K_a value of 2.05 x 10^6 M^{-2} for the association of **KRS-1** to $PrP_{106\text{-}126}$ fibrils.

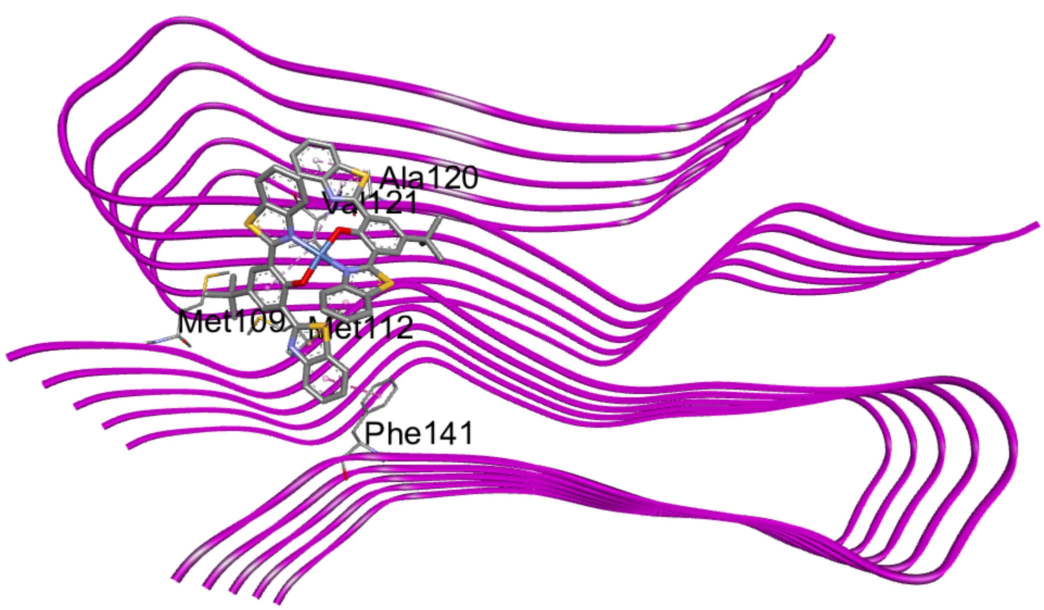

Figure S21. Stacking of **KRS-1** in square planar configuration between the β-sheets structure of prion protein fibrils.

^{94}GTHSQWNKPSKP
$_{106}$**KTNMKHMAGAAAAGAVVGGLG**$_{126}$
GYMLGSAMSRPIIHFGSDYEDRYYRE
NMHRYPNQVYYRPMDEYSNQNNFV
HD^{178}

Figure S22 The human prion protein fibril sequence of 6UUR (PDB), with prion protein fragments from 106 to 126 sequence shown in red. (The real prion sequence from 94 to 178 is indicated by superscripts).

	Name	Visible	Color	Parent	Distance	Category	Types	From	From Chemistry	To	To Chemistry
1	H:MET112:HN - d:RES1:N17	Yes		Ligand Non-bond Monitor	2.33953	Hydrogen Bond	Convention...	H:MET112:...	H-Donor	d:RES1:...	H-Acceptor
2	J:VAL121:HN - d:RES1	Yes		Ligand Non-bond Monitor	2.53429	Hydrogen Bond	Pi-Donor H...	J:VAL121:...	H-Donor	d:RES1	Pi-Orbitals
3	J:VAL121:HN - d:RES1	Yes		Ligand Non-bond Monitor	3.17906	Hydrogen Bond	Pi-Donor H...	J:VAL121:...	H-Donor	d:RES1	Pi-Orbitals
4	H:MET112:O - d:RES1	Yes		Ligand Non-bond Monitor	2.69311	Other	Pi-Lone Pair	H:MET112:O	Lone Pair	d:RES1	Pi-Orbitals
5	d:RES1:C7 - H:MET109	Yes		Ligand Non-bond Monitor	4.37446	Hydrophobic	Alkyl	d:RES1:C7	Alkyl	H:MET1...	Alkyl
6	d:RES1 - J:VAL121	Yes		Ligand Non-bond Monitor	5.33925	Hydrophobic	Pi-Alkyl	d:RES1	Pi-Orbitals	J:VAL121	Alkyl
7	d:RES1 - J:ALA120	Yes		Ligand Non-bond Monitor	4.14046	Hydrophobic	Pi-Alkyl	d:RES1	Pi-Orbitals	J:ALA120	Alkyl
8	d:RES1 - J:VAL121	Yes		Ligand Non-bond Monitor	5.32862	Hydrophobic	Pi-Alkyl	d:RES1	Pi-Orbitals	J:VAL121	Alkyl
9	d:RES1 - J:ALA120	Yes		Ligand Non-bond Monitor	4.50628	Hydrophobic	Pi-Alkyl	d:RES1	Pi-Orbitals	J:ALA120	Alkyl

Figure S23: Interaction parameters between the complex and peptide.

References:

1 L. F. Lindoy, G. V. Meehan and N. Svenstrup, *Synthesis*, 1998, 1029–1032.
2 M. Gulcan, Y. Karataş, S. Işık, G. Öztürk, E. Akbaş and E. Şahin, *J. Fluoresc.*, 2014, **24**, 1679–1686.
3 G. M. Sheldrick, *Acta Crystallogr. Sect. A*, 1990, **46**, 467–473.
4 O. V. Dolomanov, L. J. Bourhis, R. J. Gildea, J. A. K. Howard and H. Puschmann, *J. Appl. Crystallogr.*, 2009, **42**, 339–341.
5 C. F. Macrae, P. R. Edgington, P. McCabe, E. Pidcock, G. P. Shields, R. Taylor, M. Towler and J. Van De Streek, 2006, preprint, DOI: 10.1107/S002188980600731X.
6 Y. Wang, L. Feng, B. Zhang, X. Wang, C. Huang, Y. Li and W. Du, *Inorg. Chem.*, 2011, **50**, 4340–4348.
7 C. Y. Huang, *Methods Enzymol.*, 1982, **87**, 509–525.
8 Y. Li, J. Wu, X. Jin, J. Wang, S. Han, W. Wu, J. Xu, W. Liu, X. Yao and Y. Tang, *Dalton Trans.*, 2014, **43**, 1881–1887.
9 S. K. Sur, *J. Magn. Reson. 1969*, 1989, **82**, 169–173.
10 G. A. Bain and J. F. Berry, *J. Chem. Educ.*, 2008, **85**, 532–536.
11 V. Kumar, S. Haldar, S. Ghosh, S. Chauhan, A. Sharma, P. Dhankhar, A. Kumar, S. Jaiswal, S. Saini, S. Gupta, D. Lahiri and P. Roy, *Biochem. Pharmacol.*, DOI:10.1016/j.bcp.2022.115284.
12 A. D. Becke, *J. Chem. Phys.*, 1993, **98**, 5648–5652.
13 M. Frisch, G. Trucks, H. Schlegel, G. Scuseria, M. Robb, J. Cheeseman, G. Scalmani, V. Barone, G. Petersson, H. Nakatsuji, X. Li, M. Transport, A. Marenich, J. Bloino, B. Janesko, R. Gomperts, B. Mennucci, H. Hratchian and D. Gaussian, *Inc Wallingford CT*, 2016, **6**, 3977.
14 G. M. Morris, H. Ruth, W. Lindstrom, M. F. Sanner, R. K. Belew, D. S. Goodsell and A. J. Olson, *J. Comput. Chem.*, 2009, **30**, 2785–2791.
15 C. Glynn, M. R. Sawaya, P. Ge, M. Gallagher-Jones, C. W. Short, R. Bowman, M. Apostol, Z. H.

Zhou, D. S. Eisenberg and J. A. Rodriguez, *Nat. Struct. Mol. Biol.*, 2020, **27**, 417–423.
16 Y. Li, L. Wang, L. Wang, B. Zhu and J. Ma, *RSC Adv.*, 2023, **13**, 33276–33287.

-:END:-